

# Spatial Direct Numerical Simulation of Transition Phenomena in Supersonic Flat-Plate Boundary Layers

Axel Fezer and Markus Kloker

Universität Stuttgart, Institut für Aerodynamik und Gasdynamik,  
Pfaffenwaldring 21, D-70550 Stuttgart, Germany

**Abstract.** Direct Numerical Simulations (DNS) are carried out for flat-plate boundary layers at  $Ma = 2.0$  and  $6.8$  to investigate subharmonic combination-mode phenomena caused by the interaction of two three-dimensional disturbance waves with fundamental and subharmonic frequency. An unexpected long growth of the nonlinearly generated subharmonic combination mode is observed which is independent of the disturbance amplitudes. The relevance of the subharmonic modes for transition is examined by comparison with a pure oblique-type breakdown scenario.

## 1 Introduction

The investigations presented in this paper are based on an experimental study of the development of spatial wave packets induced by a hole disturbance in a flat-plate boundary layer at  $Ma = 2.0$  by Kosinov et al. [4] carried out in the supersonic wind tunnel T-325 in Novosibirsk. The simultaneous excitation of fundamental and small subharmonic 3-d disturbances led to the appearance of a strong subharmonic mode which can not be expected by Linear-Stability-Theory (LST) results. This is assumed to be the consequence of subharmonic resonance effects where a wave triplet consisting of one 3-d fundamental and two 3-d subharmonic waves (each of them determined as a peak in the  $\beta$ -spectra,  $\beta$  - spanwise wave number) meets subharmonic resonance conditions.

For our numerical simulations we disturbed pure waves, i.e. the fundamental and one subharmonic wave as two of the three relevant modes from the experiment. Since only one of the two subharmonics under consideration is linearly unstable, this mode has been chosen as disturbance input.

## 2 Numerical method

The flow is considered in a rectangular integration domain on the flat plate, not containing any shock wave induced by the leading edge. In a disturbance strip at the wall controlled disturbances are excited by timewise periodic and simultaneous blowing and suction. At the end of the integration domain a buffer domain is appended, in which all disturbances of the flow are smoothly damped to zero in order to avoid reflections from the outflow boundary.

The equation of continuity, the Navier-Stokes equations and the energy equation are used in conservative form for the variables  $\rho$ ,  $\rho u$ ,  $\rho v$ ,  $\rho w$  and  $\rho e$ , solved in a disturbance formulation. The fluid is considered as nonreacting, perfect gas, for which the thermodynamic equation of state is valid. All variables are non-dimensionalized with respect to suitable free-stream values.

In streamwise direction the spatial discretization is performed by 4<sup>th</sup>-order accurate compact finite differences with high modal resolution, which are used in a splitted form [3]. Central (viscous terms) and alternating upwind/downwind (convective terms) standard differences are used in normal direction; the grid is equidistant. In spanwise direction the flow is assumed to be periodic and symmetric, so a Fourier spectral approach

$$f(x, y, z, t) = \sum_{k=-K}^K F_k(x, y, t) e^{ik\beta z} \quad (1)$$

is used with the basic spanwise wavenumber  $\beta$ . The time integration is performed by a 4-step Runge-Kutta scheme of 4<sup>th</sup>-order accuracy. A description of the numerical method in more detail is given in [1].

### 3 Direct Numerical Simulations

Table 1 shows the parameters of the six cases discussed here. The first five cases are basically in accordance to the experiment and differ only in the chosen disturbance amplitudes  $A_{(1,4)}$  and  $A_{(1/2,3)}$ ; thereby  $(h, k)$  denotes a wave with frequency  $h \cdot F$  and the spanwise wavenumber  $\pm k \cdot \beta$ ;  $F = 2\pi f^* L / (u_\infty^* Re_L)$ ,  $\beta = \beta^* L$ ,  $L = 2.1348$  mm,  $Re_L = 10^5$ .

For Case 1, the disturbance amplitude of the subharmonic wave has been chosen ten times smaller than that of the fundamental wave. Fig. 1 shows the downstream development of the maximum amplitudes (over  $y$ ) of  $(\rho u)'$  for the most relevant modes. In addition to the directly nonlinearly generated mode (0,8) belonging to the oblique-type transition mechanism triggered by the fundamental wave (1,4), we observe a remarkably strong growth of mode (1/2,7). This mode (in the following occasionally referred to as *combination mode*) is principally generated by the two disturbed modes, but soon has greater amplitudes than the disturbed subharmonic wave. This is quite surprising at amplitudes lower than, say, 1%, but is in agreement with the experiment, where the same mode attains the highest amplitude for subharmonic disturbances. It could be conjectured that mode (1/2,7) is coupled to mode (0,8), but the suppression of (0,8) in a calculation with  $K = 7$  in ansatz (1) does not at all alter the (1/2,7) behaviour.

This raises the question whether this is a resonance mechanism requiring certain threshold amplitudes of the involved modes, or a nonlinear generation working at any amplitude level. The plot of the phase speeds in  $x$ -direction (Fig. 3) reveals that there is no special synchronization mechanism. However,

the wave vectors form a closed triad both in the  $F$ - $\beta$  and  $\alpha$ - $\beta$  plane ( $\alpha$  is the streamwise wave number and  $c_{ph,x} = \beta/\alpha$ ). Therefore we bring up Case 2 where the modes are disturbed at very low amplitudes, two orders of magnitude smaller than in Case 1 for each mode. Consequently the initial amplitude of mode  $(1/2,7)$  (not shown here) is four orders of magnitude smaller than in Case 1, but the amplification rates are exactly the same (Fig. 4; deviations occur not until amplitudes get strongly nonlinear in Case 1). So we conclude that the growth rate of this subharmonic mode is not dependent on the amplitude level but solely on the amplification rates of the generating modes, like the behaviour of the vortex mode in the pure oblique-type scenario. From Fig. 4 we can also see why  $(0,8)$  is more amplified than  $(1/2,7)$ : The generating modes  $(1,\pm 4)$  for the first are more amplified than  $(1,\pm 4)$  and  $(1/2,\mp 3)$  for the latter. Moreover, the growth rates of the generated modes are clearly higher than just the growth-rate sum of the generating modes (superquadratic nonlinearity), unlike the almost quadratic incompressible behaviour.

What about the role of the subharmonic modes for the laminar-turbulent breakdown? The growth of  $(0,8)$ ,  $(1,12)$  etc. in Case 1 shows that oblique breakdown is initiated by mode  $(1,4)$ . The considered subharmonic modes remain one order of magnitude smaller, so their influence on the breakdown mechanism is small. For investigation of the role of the initial amplitude level we successively increased the disturbance amplitude of the subharmonic wave  $(1/2,7)$  with respect to the fundamental wave in Cases 3 and 4. As a consequence  $(0,8)$  and  $(1/2,7)$  are comparably strong in Case 3 (Fig. 2). In addition to the stationary and fundamental modes of the pure oblique-type breakdown scenario we now have competitive subharmonic modes  $(1/2,7+k\cdot 4)$  (we remark that other possible modes like  $(1/2,1)$  or  $(11/2,7)$  etc. play no dominant role and are omitted in the plots). As expected, in Case 4 mode  $(0,8)$  is four times smaller than in Case 3, whereas the subharmonic mode  $(1/2,7)$  keeps its level.

It remains to examine whether the structures which lead to transition are different from that of a pure oblique-type breakdown. For this purpose we compare Cases 3 and 4 with a simulation where the subharmonic modes are completely absent (Case 5), i.e. a pure oblique-type transition scenario. First we can state that in Case 3 the modes leading to oblique breakdown are virtually untouched from the existence of the subharmonic modes (Fig. 5). So we can at best expect a subharmonic transition process running in competition with oblique breakdown. Fig. 6 shows a comparison of the spanwise vorticity ( $\omega_z$ ) iso-contours at two planes  $x = \text{const.}$  for Cases 4 and 5. Case 5 (Fig. 6a) shows the known structure of oblique breakdown. The simulation domain includes four spanwise wave lengths of  $(1,4)$ , so eight maxima are visible close to the wall and in the outer boundary-layer part as spanwise cuts of the staggered asparagus-type structures. In Case 4 (Fig. 6b) packages of four maxima form within one spanwise period which are, going downstream, periodically shifted about half a basic spanwise wavelength. The most intense shear layers periodically appear at  $z/\lambda_z \approx \frac{7}{16}, \frac{9}{16}$  and  $z/\lambda_z \approx \frac{1}{16}, \frac{15}{16}$ ,

respectively. Although the amplitudes of the subharmonic modes are about as strong as the fundamental modes in Case 5, the resulting structures are weaker. If we extrapolate these results to Case 3 which is somewhat in between Case 4 and Case 5, we can expect that the shown structures overlay each other. Starting from Case 5, this should mainly concern the shear-layer  $z$ -positions mentioned for Case 4 above. Fig. 7a (Case 5) and 7b (Case 3) show planes  $z = \text{const.}$  near and at  $z = \frac{1}{16} \cdot \lambda_z$ . It can clearly be seen that in this plane the shear-layer close to the wall downstream of  $x = 8.5$  is strengthened significantly (Fig. 7b), whereas the planes around look similar than in Fig. 7a. This fact is confirmed by the curves of the local skin friction coefficient  $c_f$  or the shape parameter  $H_{12}$  in Fig. 8, where the values of Case 3 deviate earlier from the laminar values. This means that the subharmonic modes can accelerate oblique breakdown.

From the view of LST the most unstable wave should refer to the fundamental wave in our simulation. This mode triggers oblique breakdown. An additional (smaller) subharmonic wave generates the combination mode, but as shown above, its amplification rate will be smaller than that of the vortex mode. Hence, breakdown as a direct consequence of a subharmonic combination mechanism is, compared to oblique breakdown, rather unlikely and will never appear separately. Note that Kosinov et al. [4] did not include in their discussion the typical oblique-type scenario vortex mode inevitably generated by the fundamental mode. However, oblique breakdown can additionally be enriched by the presence of subharmonic modes.

Furthermore, in Case 6 we examined if the growth of the combination mode also takes place in a boundary layer at hypersonic speed ( $Ma = 6.8$ , flight conditions with cooled wall  $T_w = 975$  K, for details see [2]). Fig. 9 shows that at these conditions we largely have the same behaviour as in Case 1. The disturbance modes (first-mode disturbances in the sense of LST) were not adapted to a special case, so we think that the combination mode will appear in any case.

## 4 Conclusions

Disturbing a 3-d fundamental and a 3-d subharmonic wave with different spanwise wave numbers in a supersonic flat-plate boundary layer causes an unexpected long growth of a nonlinearly generated combinational subharmonic wave, with growth properties similar to the stationary vortex mode in the pure oblique-type scenario and no dependency of the vortex mode. Since the combination mode is instationary, its behaviour cannot be easily explained by the “lift-up effect”. However, the growth rates of corresponding subharmonic modes are not larger than those of the fundamental modes, so standard oblique-type breakdown modes are likely to dominate. But the simulations also show that oblique breakdown can be accelerated by the presence of subharmonic disturbances. The examinations also showed that this occurrence is neither dependent on the exact choice of the disturbed waves nor on

the flow properties, so the same phenomena could be found at  $Ma = 2.0$  and  $Ma = 6.8$ .

The financial support of the Deutsche Forschungsgemeinschaft, DFG, within SFB 259, TP C4, is gratefully acknowledged.

## References

1. H. Bestek and W. Eißler. DNS of Transition in Mach 4.8 Boundary Layers at Flight Conditions. In G. Bergeles W. Rodi, editor, *Engineering Turbulence Modelling and Experiments 3*. Elsevier Science B.V., 1996.
2. A. Fezer and M. Kloker. Transition processes in Mach 6.8 boundary layers at varying temperature conditions investigated by spatial direct numerical simulation. In W. Nitsche and R. Hilbig, editors, *Notes on Numerical Fluid Mechanics*. 11<sup>th</sup> Stab Symposium 98, Berlin, Vieweg Verlag, 1999.
3. M. Kloker. A Robust High-Resolution Split-Type Compact FD-Scheme for Spatial Direct Numerical Simulation of Boundary-Layer Transition. In *Applied Scientific Research 59 (4)*, pages 353–377. Kluwer Acad. Publishers, NL, 1998.
4. A.D. Kosinov, N.V. Semionov, S.G. Shevelkov, and O.I. Zinin. Experiments on the nonlinear instability of supersonic boundary layers. In S.P. Lin, W.R.C. Phillips, and D.T. Valentine, editors, *Nonlinear Instability of Nonparallel Flows*, pages 196–205. Springer-Verlag, Berlin, 1993.

**Table 1.** Simulation parameters

	Case 1	Case 2	Case 3	Case 4	Case 5	Case 6
$Ma_\infty$	2.0	2.0	2.0	2.0	2.0	6.8
$F \cdot 10^5$	3.8	3.8	3.8	3.8	3.8	2.0
$\beta$	3.03	3.03	3.03	3.03	3.03	1.4
$A_{(1,4)}$	$1 \cdot 10^{-3}$	$1 \cdot 10^{-5}$	$1 \cdot 10^{-3}$	$5 \cdot 10^{-4}$	$1 \cdot 10^{-3}$	$2.5 \cdot 10^{-3}$
$A_{(1/2,3)}$	$1 \cdot 10^{-4}$	$1 \cdot 10^{-6}$	$1 \cdot 10^{-3}$	$2 \cdot 10^{-3}$	0.0	$2.5 \cdot 10^{-4}$

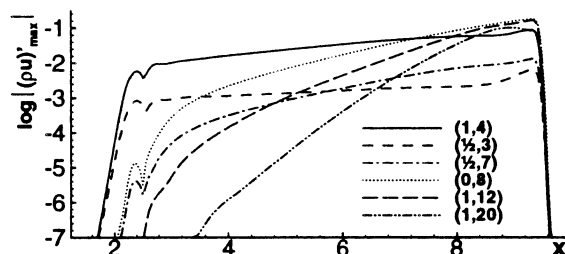


**Fig. 1.** Downstream development of the  $|(\rho u)'_{(h,k)}|$  disturbance amplitudes; Case 1

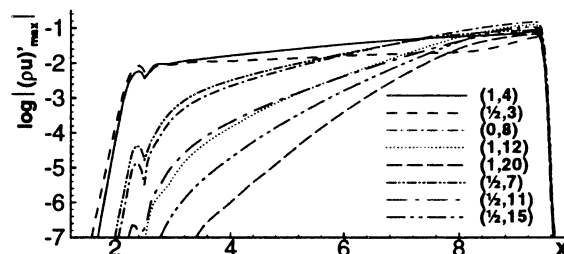


**Fig. 2.** Downstream development of the  $|(\rho u)'_{(h,k)}|$  disturbance amplitudes; Case 3

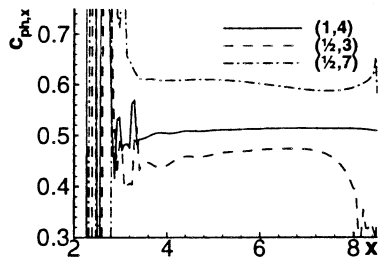


**Fig. 3.** Phase speed of several modes; Case 1

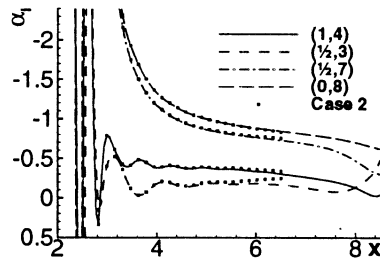


**Fig. 4.** Amplification rates of several modes for Case 1 (lines) and Case 2 (symbols)

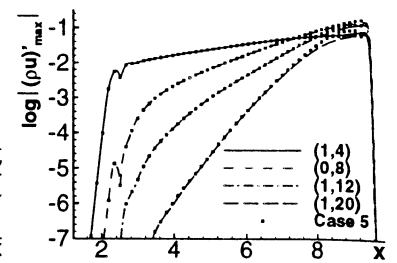


**Fig. 5.**  $|(\rho u)'_{(h,k)}|$  disturbance amplitudes for Case 3 (lines) and Case 5 (symbols)

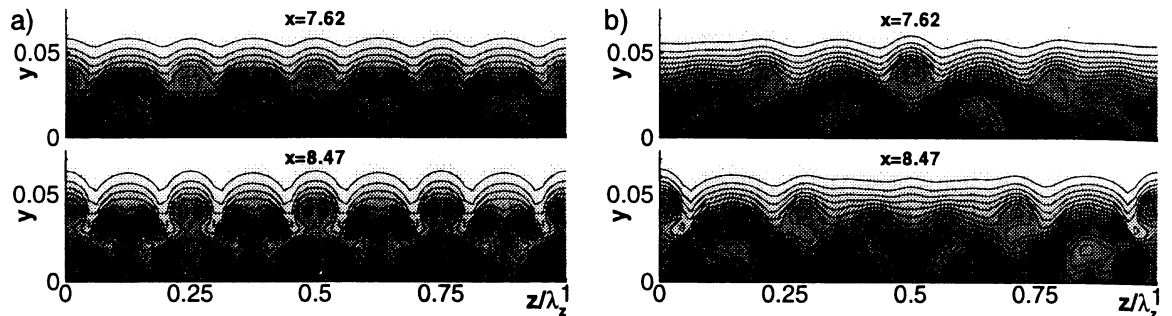


**Fig. 6.** Isocontours of instantaneous total spanwise vorticity  $\omega_z$ . a) Case 5 b) Case 4

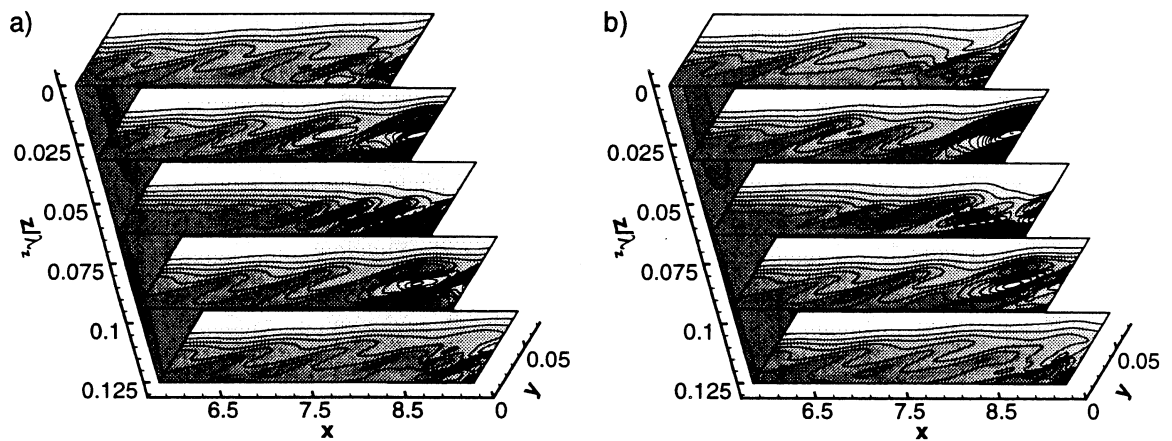


**Fig. 7.** Isocontours of the instantaneous total spanwise vorticity  $\omega_z$  at several  $z$ -positions. a) Case 5 b) Case 3

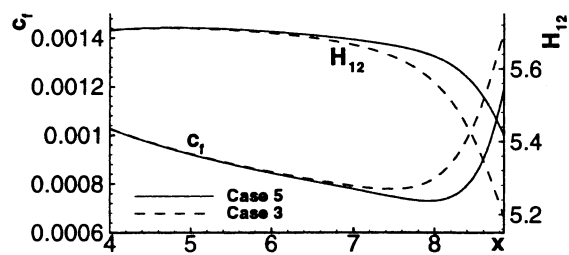


**Fig. 8.** Local skin friction coefficient  $c_f$  at  $z = \frac{1}{16} \lambda_z$  and averaged shape parameter  $H_{12}$

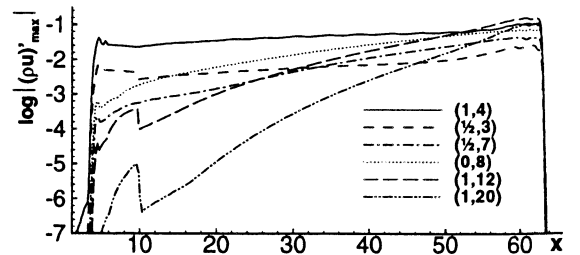


**Fig. 9.** Downstream development of the  $|(\rho u)'_{(h,k)}|$  disturbance amplitudes; Case 6